Nodal Photolithography: Lithography via Far-Field Optical Nodes in the Resist

by

Donald Winston

Submitted to the Department of Electrical Engineering and Computer Science
in partial fulfillment of the requirements for the degree of

Master of Science in Electrical Engineering and Computer Science

at the

MASSACHUSETTS INSTITUTE OF TECHNOLOGY

February 2008

© Massachusetts Institute of Technology 2008. All rights reserved.

Author . . . .
Department of Electrical Engineering and Computer Science
January 18, 2008

Certified by . . . .
Karl K. Berggren
Associate Professor
Thesis Supervisor

Accepted by . . . .
Terry P. Orlando
Chairman, Department Committee on Graduate Students

Nodal Photolithography: Lithography via Far-Field Optical Nodes in the Resist

by

Donald Winston

Submitted to the Department of Electrical Engineering and Computer Science
on January 18, 2008, in partial fulfillment of the
requirements for the degree of
Master of Science in Electrical Engineering and Computer Science

Abstract

In this thesis, I investigate one approach – stimulated emission depletion – to surmounting the diffraction limitation of optical lithography. This approach uses far-field optical nodes to orchestrate reversible, saturable optical transitions in certain photoresist compounds. After addressing prior work in resolution enhancement via optical nodes (for metastable atom localization, reversible absorbance modulation, and fluorescence microscopy), I examine the issues of resist formulation, optical pulse width bounds due to resist kinetics, and patterning schemes for low- and high-volume throughput. The experimental realization of stimulated emission depletion is described, and challenges for lithography using this technique are discussed.

Thesis Supervisor: Karl K. Berggren
Title: Associate Professor

Acknowledgments

I first of all thank Karl. You helped me select the topic of this thesis, you provided guidance for it throughout, and more generally you ensured (and continue to ensure) a research environment conducive to my well-being and to that of my labmates. Liz Young, your patience and experience has made experimental work much less frustrating than I had feared; in fact, it's been fun. Steve Kooi, your expertise in ultrafast lasing and your volunteering of experimental time and space was gracious. Kris Rosfjord, your early presence in this project made my transition from earlier work much easier than I had anticipated; your continued help, even after you sailed off to junior faculty land, was much appreciated and inspiring. Adam Chao, friend, roommate, UROP, your skill in the cleanroom is matched only by your skill at that computer game you nestle into each evening. I also thank my family for nature and nurture; my friends – particularly the "cookie monday" crew – for steady encouragement, cherished recreation, and shared advice; and Emily, mi gordita, for your set of supportive acts with cardinality greater than that of the natural numbers.

Contents

1 Resolution ↑ and Cost ↓ with Optical Nodes **11**

1.1 The Art of Optical Lithography Approaches Natural Limits 12

1.2 Resolution Increase Through A Reversible and Saturable Optical Transition 13

2 Resolution Enhancement via Optical Nodes: Prior Work **17**

2.1 Metastable Atom Localization at the Heisenberg Limit 17

2.2 Reversible Absorbance Modulation Layers 20

2.3 Stimulated-Emission-Depletion Microscopy 21

2.3.1 The Photophysical Model of a Fluorophore 22

2.3.2 Review of Contributions to Resolution Enhancement in Microscopy 25

3 Considerations for a Nodal Lithography System **27**

3.1 Resist Formulation Depends on Applicability of Existing Systems . . 27

3.1.1 Existing Resists 28

3.1.2 Sensitization of Existing Resists 29

3.1.3 Modular Approach: PAC Insertion Into Known Resin Systems 31

3.1.4 Synthesis of Designed PAC/resin System 31

3.2 Optical Pulse Width Bounded By Resist Kinetics 34

3.2.1 Ti:Sapphire System with Pulse Stretching for Fast Kinetics . . 34

3.2.2 Diode System for Not-as-Fast Kinetics 35

3.2.3 CW Sources for Photoreversible Resists 35

3.3 Patterning Scheme Determined by Throughput Requirements 35
3.3.1 Serial Direct-Write for Low Throughput 35
3.3.2 Double Exposure Interference Lithography for High Throughput 37

4 Experimental Realization of STED 39
4.1 Generate and Synchronize Excitation Pulses and STED Pulses 39
4.1.1 Self-mode-locking in a Ti:sapphire System 40
4.1.2 Correcting Group Velocity Dispersion (GVD) 41
4.1.3 Pulse Picking with a Pockels Cell 41
4.1.4 Chirped Pulse Amplification (CPA) 42
4.1.5 Second Harmonic Generation (SHG) 42
4.2 Choose a Material Under Test for Concurrent Verification 43
4.2.1 High Fluorescence Yield 43
4.2.2 Photostability 44
4.2.3 Large Cross-section for Stimulated Emission 44
4.3 Position and Focus Pulses Appropriately 44
4.3.1 Excitation Volume Enclosed by STED Volume 45
4.3.2 Too-Tight STED Pulse Focus Causes Continuum Generation . 46
4.4 Track Pulse Spacing and Verify STED with a Streak Camera 47
4.4.1 Tracking of Interpulse Spacing for Delay Guidance 47
4.4.2 Verification of STED 48
4.5 Stretch. . . or Do Not Stretch 49
4.5.1 STED is Achieved with “Native” Pulse Width 50
4.5.2 Stretching is Advantageous if Allowed by Material Kinetics . . 50

List of Figures

1-1 Markov chain model of a photoactive molecule 13

2-1 Chemical change versus dose 18

2-2 The proximity effect 19

2-3 Energy levels in a photoactive compound 22

2-4 The Franck-Condon principle 23

2-5 Excited state types: singlet versus triplet 23

2-6 Dependence of internal conversion efficiency on state energy separation 24

3-1 Energy level diagram for triplet sensitization 29

3-2 Photoinduced electron transfer 30

3-3 Examples of vinyl polymers 33

3-4 Step-and-repeat or scan for low throughput 36

3-5 A potential nodal lithography system 36

3-6 3D patterning 37

4-1 System used for pulse generation 40

4-2 Integrated system for STED verification 46

4-3 Elements of a streak camera 47

4-4 Streak camera integrations without and with the STED pulse 48

Chapter 1

Resolution ↑ and Cost ↓ with Optical Nodes

Light-based integrated circuit manufacturing tools are widely used in research on micro- and nano-scale phenomena. These tools are economical for high-volume production, but basic research is low-volume and its yield requirements are less stringent. Still, researchers insist on these tools for cutting-edge investigation because they present the best patterning resolution possible without inflicting substrate damage as in electron and ion beam lithography.

Cost per function has traditionally decreased in IC manufacturing because increases in resolution have outpaced increases in tool costs. However, tool costs are escalating, and given that device critical dimensions are now a mere two orders of magnitude greater than atomic dimensions, it is not clear that significant resolution enhancement can be done economically.

Lithography via far-field optical nodes in the resist – or nodal photolithography – can decrease the cost of photo-patterning in research without sacrificing resolution, and it can decrease cost per function for integrated circuit manufacturing, through eliminating the need for precision mask generation and alignment. Mask-less direct writing for low-volume research and double-exposure interference lithography with trim masks for high-volume manufacturing, both of which are discussed in detail in Section 3.3, can advance the art of far-field photolithography.

1.1 The Art of Optical Lithography Approaches Natural Limits

Currently, resolution in far-field optical lithography is limited by diffraction of the light that writes. The point spread function of an ideal write beam is the Airy pattern, and resolution in such a system is set by the $\propto \lambda/(2\,\mathrm{NA})$ center-to-center separation of Airy disks, where λ is the wavelength of the light and NA is the numerical aperture of the focusing system.

To achieve better resolution, lithographers have scaled both wavelength and numerical aperture, but practical limits exist. At $\lambda = 157$nm, many molecules like oxygen, water, and most organic compounds are opaque; this hampers photoresist action, increases contamination, and frustrates design of the mask pellicle and of the lens elements [1]. Consequently, the $\lambda = 193$nm ArF laser continues its reign in industry. Regarding numerical aperture, the $n = 1.44$ refractive index of water at 193nm limits water-immersion systems to NA < 1.44. One estimate on the NA limit under 193nm illumination that considers higher-index immersion fluids is NA $= 1.55$, limited by the $n = 1.56$ index of fused quartz lens elements [2]; it is difficult to find a higher projected value in the literature.

An all-encompassing k_1 value is used to characterize the combined effect, distinct from the effect of scaling wavelength and numerical aperture, of various resolution enhancement techniques (RET). Thus, resolution is equal to $k_1 \frac{\lambda}{\mathrm{NA}}$ for a given lithographic process. Example RETs include phase-shifting masks, optical proximity correction (OPC), off-axis illumination with OPC, polarized illumination, and double exposure/patterning. k_1 today is as low as 0.4 for logic circuits and 0.35 for memory circuits. One estimate for a future k_1 that requires the split-pitch technique (double exposure/patterning) is 0.15; with $\lambda = 193$nm and NA $= 1.55$, this corresponds to 19nm half-pitch [2].

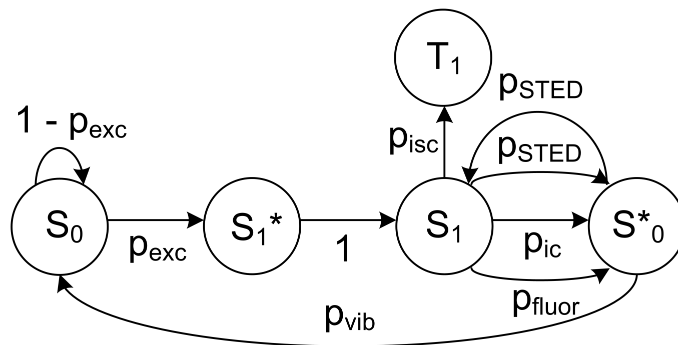

Figure 1-1: A Markov chain model of a photoactive molecule that can help describe the general idea of a reversible and saturable optical transition. The state T_1 is modeled as a terminal state, and the use of a Markov model is inappropriate other than for preliminary instruction because, via the photobleaching effect, arrival at future states *does* depend on state history. See the introductory paragraph of Section 1.2 for a walk-through of this figure.

1.2 Resolution Increase Through A Reversible and Saturable Optical Transition

A reversible and saturable transition may be understood via a simplistic Markov model as in Figure 1-1. A photoactive molecule initially in the (vibrationally-relaxed) singlet ground state S_0 has a certain probability p_{exc} to absorb an incident photon and thus transition to a vibrationally-unrelaxed excited singlet state S_1^*. Vibrational relaxation then occurs rapidly, illustrated by a transition to state S_1. Without the presence of an induced stimulated-emission-depletion (STED) transition (i.e., $p_{STED} = 0$), the molecule will transition to either the triplet state T_1, which is modeled as a dead end for reasons that are explained in Section 3.1.1, or to the vibrationally-unrelaxed ground singlet state S_0^*, which precedes in this case certain vibrational relaxation. However, if p_{STED} far exceeds the probabilities of intersystem crossing (p_{isc}), internal conversion (p_{ic}), and fluorescence (p_{fluor}), while remaining much less than the probability of vibrational relaxation (p_{vib}) within the ground state singlet manifold, then the particular optical transition $S_1 \xrightarrow{p_{STED}} S_0^*$ is saturated. This saturable induced transition also represents the potential reversibility of, for example, a likely $S_1 \xrightarrow{p_{isc}} T_1$ transition in a situation where $p_{isc} \gg p_{ic} + p_{fluor}$, which is indeed the situation in

photoresists.

Nodal photolithography uses a reversible, saturable optical transition in photoresist to reduce the effective point spread function of exposure. The photophysics of photoactive molecules is reviewed in Section 2.3.1. Let

$$p_{exc}(x) = cos^2\left(2\pi x \frac{sin\alpha}{\lambda_{exc}}\right)$$

be a diffraction-limited probability distribution for excitation of photoresist in the focal plane of a $\lambda = \lambda_{exc}$ light pulse. With α being the half-angle between two mutually coherent beams directed at the photoresist surface, and with x being the position along the appropriate axis, this distribution is recognized as a standing wave. Excitation is to a singlet state, and subsequent intersystem crossing to a triplet state is required for chemical change. Given the intersystem crossing rate k_{isc}, if a second pulse of duration $\tau \ll 1/k_{isc}$ were to deplete the singlet state via stimulated emission, then the photoresist should not undergo chemical change. This assumes $\tau \gg \tau_{vib}$, where τ_{vib} is the vibrational relaxation time within a singlet manifold; otherwise, re-excitation would be a problem. Also, the rate of stimulated emission depletion k_{STED} must far exceed the rates of both radiative (fluorescence) and nonradiative (internal conversion) transitions back to the ground state.

Since $k_{STED} \gg k_{isc}$, the probability that excited photoresist remains active after a STED pulse hits it is given by

$$\eta(x) = e^{-\tau \cdot k_{STED}(x)} \equiv e^{-\sigma\tau I_{STED}(x)},$$

where σ is the molecular cross-subsection for stimulated emission, and $I_{STED}(x)$ is the intensity at position x of $\lambda = \lambda_{STED}$ light. Defining $I_{sat} \equiv \frac{1}{\sigma\tau}$ and $\zeta \equiv I_{max}/I_{sat}$, where I_{max} is the maximum value of $I_{STED}(x)$, consider

$$I_{STED}(x) = \zeta I_{sat} sin^2\left(2\pi x \frac{sin\alpha}{\lambda_{STED}}\right)$$

as a diffraction-limited standing wave representing the intensity of a $\lambda = \lambda_{STED}$ STED

pulse. Its peaks correspond to the nodes of the excitation pulse. Due to vibrational relaxation within the ground and excited singlet manifolds, $\lambda_{STED} > \lambda_{exc}$; however, for this derivation, suppose $\lambda_{STED} = \lambda_{exc} \equiv \lambda$. The probability to undergo chemical change at position x is thus given by

$$p(x) = p_{exc}(x)\eta(x) = cos^2 A \cdot e^{-\zeta sin^2 A},$$

where $A \equiv 2\pi x \frac{nsin\alpha}{\lambda}$.

The FWHM can be estimated from Taylor expansion; this requires $x \ll \frac{\lambda}{2n}$ such that A is small.

$$\begin{aligned}
cos^2 A &\approx (1 - \frac{1}{2}A^2)(1 - \frac{1}{2}A^2) \approx 1 - A^2 \\
e^{-\zeta sin^2 A} &\approx 1 - \zeta sin^2 A \approx 1 - \zeta A^2 \\
\Rightarrow h(x) &\approx (1 - A^2)(1 - \zeta A^2) \approx 1 - A^2 - \zeta A^2 = 1 - (1 + \zeta)\left(2\pi x \frac{nsin\alpha}{\lambda}\right)^2 \\
\Rightarrow \text{FWHM} &= 2 \cdot [x]_{h(x)=1/2} = \frac{\sqrt{2}}{\pi} \cdot \frac{1}{\sqrt{1+\zeta}} \cdot \frac{\lambda}{2nsin\alpha}
\end{aligned}$$

Since the FWHM decreases by an adjustable factor of $\approx \sqrt{1 + I_{max}/I_{sat}}$, resolution is enhanced both by increasing STED pulse intensity and by decreasing photoresist saturation intensity. Since $I_{sat} = \frac{1}{\sigma\tau}$, saturation intensity can be decreased by using photoactive compounds that either are more efficient at stimulated emission (σ increases), or are more stable in the excited singlet state (so that τ can be increased).

The fundamental geometric requirements for the technique are twofold: first, that the outer surface of the STED pulse's focal volume encompasses that of the excitation pulse; and second, that a node must exist in the field of the STED pulse. This causes intersystem crossing of the photoactive compound in the resist and thus chemical change to be localized at this node, assuming the node coordinates are within the excitation pulse volume. Because the pattern transferred to the resist is defined by nodes, this technique has been named "nodal photolithography".

Nodal lithography has numerous benefits as a resolution enhancement technique. It uses far-field illumination, avoiding the depth dependence of near-field techniques.

With appropriate pulse shaping, it patterns in three dimensions. It is not diffraction-limited, so light of $\lambda > 193$nm is fine; this is important because the $\lambda = 193$nm ArF laser may not be able to output enough intensity for significant resolution enhancement at low cost (this is why chemically-amplified resists are used in industry). Finally, since resolution in nodal lithography depends on the *ratio* I_{max}/I_{sat}, any practical limit on STED pulse intensity does not correspond to a practical limit on resolution; a metastable singlet state would enable $I_{sat} \to 0$ and thus $k_1 \to 0$.

Chapter 2

Resolution Enhancement via Optical Nodes: Prior Work

Resolution enhancement via far-field optical nodes has been accomplished for neutral atom deposition [3], but this approach has limited applicability. Also, optical nodes have been used to aperture a contrast enhancement layer [4], but this approach does not actually break the diffraction limit (see Section 2.2 for details). Finally, imaging via optical nodes was only demonstrated less than a decade ago, and the requirements for resist patterning are more stringent.

2.1 Metastable Atom Localization at the Heisenberg Limit

K.S. Johnson et. al. were able to deposit etch-resistant material on a substrate at the nodes of an optical standing wave, with feature sizes as small as 20nm [3]. Patterning at spatial frequencies higher than the diffraction-limited spatial frequency of the standing wave, via suitable stage displacement, is possible because the rate of the chemical change that causes deposition of their resist monotonically decreases with exposure dose. This is unlike optical interference lithography in a traditional photoresist; in a traditional photoresist, chemical change monotonically increases with

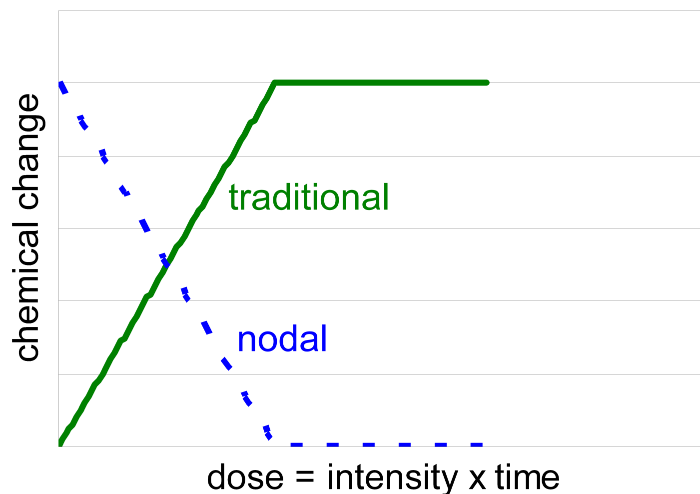

Figure 2-1: Chemical change in a traditional resist monotonically increases with dose and saturates at 100% chemical change, whereas chemical change in a nodal resist monotonically decreases with dose and saturates at zero chemical change.

exposure dose (see Figure 2-1).

Because the relationship between chemical change and dose is not a step function, a *proximity effect* limits the minimum distance between printed features. Figure 2-2 may help to visualize this. The two beams centered at $x = \pm a$ impart chemical change at each point X (ignoring resist depth) proportional to the density of blue dots along the line $x = X$. Assuming an ideal step function relationship between development and chemical change[1], development occurs if and only if chemical change is above some threshold. If an additional beam is centered at $x = 0$, it is unclear that three distinct features will develop; the individual sub-threshold intensities of adjacent beams at various points may add to above-threshold values at those points. Even if the beams are not "on" at the same time, the resist has memory: dose = intensity $\times$ time.

In the nodal lithography of [3], chemical change has an exponential relationship with dose because the metastable atoms undergo fast exponential decay to the atomic ground state (after excitation to a higher-energy state) in the high-field regions of a resonant optical standing wave. At the optical nodes on the substrate surface, the

[1]justified because a more realistic portrait of this relationship would not yield any additional distinction between traditional and nodal resists

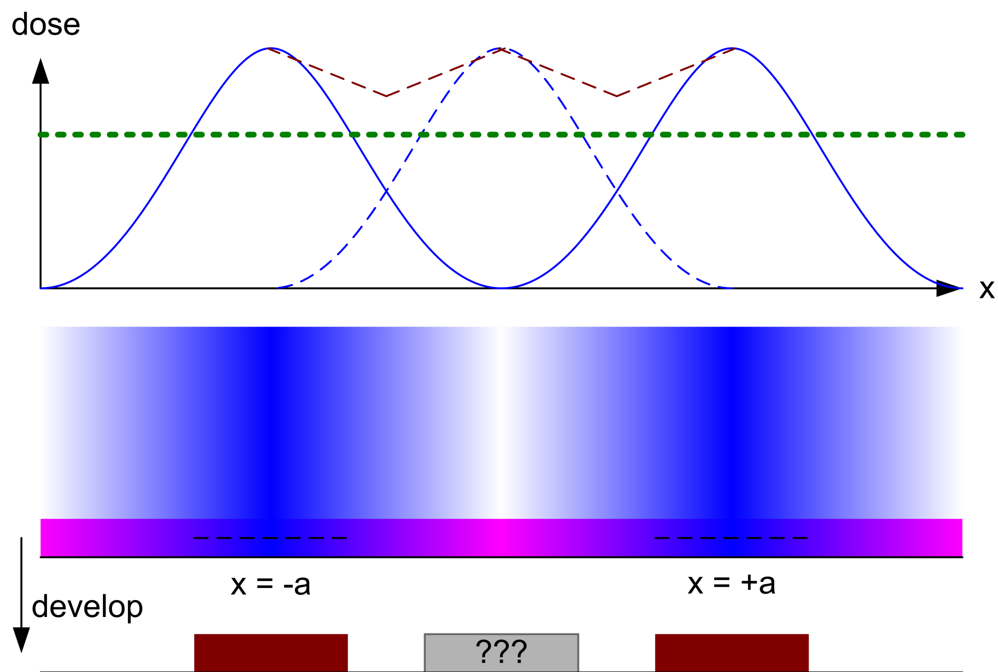

Figure 2-2: A proximity effect limits the minimum distance between developed features. Chemical change is depicted as varying linearly with dose in the resist. The dotted lines span values of chemical change that are above the threshold for development. If a third beam that centered on $x = 0$ was introduced, the proximity effect could result in one long (length $> 2a$) feature rather than three features.

metastable atoms give energy to a hydrocarbon vapor that permeates the chamber. This energy transfer results in the deposition of a carbonaceous film on the substrate at these nodes. Thus, the standing wave pattern acts as an absorption grating that gates chemical change rather than physical penetration.

However, this process has limitations. Whereas traditional photoresist is a spin-on polymeric film that is static prior to exposure, the carbonaceous resist is a gas that deposits *during* exposure. Because of this, optical diffraction is merely replaced by matter wave diffraction as a limitation on resolution; the metastable atoms localized at optical nodes wander according to Heisenberg uncertainty. Apart from resolution concerns, this process has a very slow deposition rate – the authors report a total deposition thickness of 0.6 ± 0.3nm.

2.2 Reversible Absorbance Modulation Layers

A layer of photochromic material spun over photoresist has been used to provide sub-wavelength apertures for light on its way to the photoresist [4]. The technique employs two lasers of different wavelengths – one (400-nm) induces transparency in the photochromic layer and exposes the resist, whereas the other (532-nm) hinders transparency in the photochromic layer and falls outside the absorption band of the resist. When a uniform flood exposure of 400-nm light is superimposed upon a larger-peak-intensity standing wave pattern of 532-nm light, a dynamic competition ensues within the photochromic layer. The steady-state result is an absorption grating in which the apertures are centered at the nodes of the 532-nm standing wave.

The width of an aperture is not in direct proportion to either the wavelength of the transparency inducer or that of the transparency inhibitor; rather, it scales as the *ratio of the intensities* of the two light sources – the higher the ratio $I_{inhibitor}/I_{inducer}$, the smaller the aperture. Thus, aperture size is not diffraction-limited.

To pattern at a spatial frequency beyond the diffraction limit, the photochromic layer must be "reset" via a long (20-minute) exposure to only the 532-nm light. Only then, and after repositioning the substrate relative to the light sources, may the layer

be re-exposed to 400-nm light. In this way, assuming that photoresist exposure line widths scale as photochromic layer aperture widths, multiple-exposure patterning is possible without multiple development and etch steps.

Unfortunately, this scheme does not actually eliminate the effect of diffraction on attainable resolution – it merely sweeps it under a rug, and that rug is the photochromic layer. Light diffracts after passing through slits, and the dynamic slits of this layer are no exception. Since chemical change in the resist has a linear relationship with dose, internal diffraction feeds the proximity effect, which in turn limits resolution. Also, unrelated to resolution but worth mentioning, diffraction within the resist limits aspect ratio.

The resolution limit imposed by diffraction in the resist after aperturing may be approximated by imagining that a one-dimensional aperture of width w is in the focal plane of a lens, so that $w = 1.22\lambda\frac{f}{D}$, where λ is the wavelength of light used, f is the imagined lens' focal length, and D is the imagined lens' diameter. Moving a distance $f = d_{2\times}$ away from the aperture into the resist such that the beam waist doubles, this means that $D = 2w$. Thus,

$$w = 1.22\lambda\frac{f}{D} = 1.22\lambda\frac{d_{2\times}}{2w} \Rightarrow d \approx \frac{2w^2}{1.22\lambda}\,.$$

With a resist thickness of 50nm and $\lambda = 400$nm light, diffraction limits w and thus feature width to 110nm.

2.3 Stimulated-Emission-Depletion Microscopy

In 1994, S.W. Hell and J. Wichmann published a theory for resolution enhancement in fluorescence microscopy [5]. They modeled a fluorescent molecule, or fluorophore, as a system of two energy states. Each of the two energy states is a manifold of vibrational levels. The rate equations for transitions between levels in such a system were analyzed to determine under what conditions stimulated emission could compete with fluorescence, or spontaneous radiative decay. Section 1.2 derives the

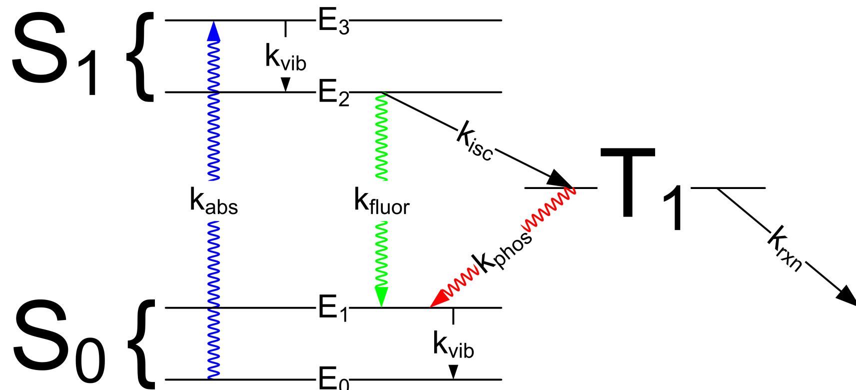

Figure 2-3: *Energy Level Diagram.* For simplicity, only the highest and lowest vibrational levels of each singlet state are depicted. Wavy lines denote radiative transitions – absorption (abs), fluorescence (fluor), and phosphorescence (phos); straight lines denote non-radiative transitions – vibrational relaxation (vib), intersystem crossing (isc), and chemical reaction (rxn). Many possible transitions and states are omitted, both to reduce clutter and because, as explained in the text, their influence can be ignored.

resolution enhancement achieved when such conditions are satisfied and when intersystem crossing to a third, triplet, energy state is significant. The photophysical model of a fluorophore will now be discussed, followed by a review of the contributions STED has made to resolution enhancement in microscopy.

2.3.1 The Photophysical Model of a Fluorophore

Various constraining relationships among the transition rates depicted in the energy level diagram of Figure 2-3 are significant for STED. For example, the Franck-Condon principle states that the absorptive transition with the highest probability is that for which the ground and excited states have minimum (spatial) geometric difference (See Figure 2-4) [6]. Correspondingly, absorption typically occurs over $\tau_{abs} \sim 10^{-16}$ to 10^{-14} seconds, whereas vibrational relaxation typically occurs over $\tau_{vib} \sim 10^{-12}$ to 10^{-11} seconds. It is important to include this phenomenon in the model because it places an upper bound on the engineered rate k_{STED} for efficient stimulated emission depletion: $k_{STED} < 1/\tau_{vib}$.

Excitation is generally to a singlet state, meaning the electron excited to a higher

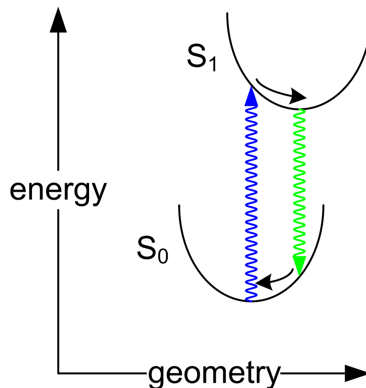

Figure 2-4: *The Franck-Condon principle.* The absorptive transition with the highest probability is that for which the ground and excited states have minimum geometric difference.

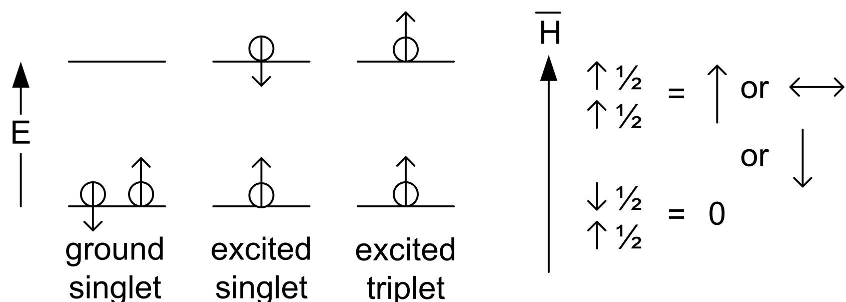

Figure 2-5: *Excited State Types: Singlet versus Triplet.* In the ground state, both electrons are in a low-energy orbital and have opposite spin due to Pauli exclusion. Because the ground state electrons are of opposite spin, this state is a singlet state. Upon excitation, a higher-energy orbital receives an electron. There is initially no spin flip of the excited electron, so this excited state is a singlet state. By Hund's rule, one may expect a spin flip to be energetically favorable, so transforming the excited state to a triplet state is possible. The singlet and triplet states are so named because of their behavior in a magnetic field. The two electron spins of a triplet state combine constructively in the presence of a magnetic field, yielding net spin either parallel to the field, anti-parallel to the field, or perpendicular to the field. The term 'triplet' refers to this three-fold degeneracy. The two electron spins of a singlet state combine destructively; the term 'singlet' refers to the absence of degeneracy.

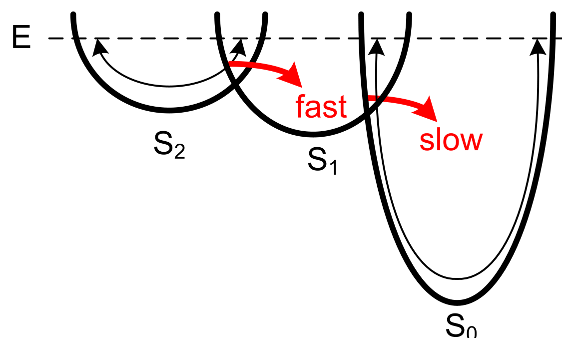

Figure 2-6: *Dependence of Internal Conversion Efficiency on State Energy Separation.* Assuming simple harmonic oscillation, an isoenergetic transition results in a change in oscillation frequency (the dashed line represents the system's total energy). A system vibrating slowly generally does not start vibrating rapidly, so internal conversion to a given state from one of much higher energy is unlikely; in order words, its transition rate is very small.

energy level does not undergo a spin flip. Because of the spin flip needed, excitation directly to a triplet state is $\sim 10^3$ to 10^6 times less efficient than excitation to a singlet state [7]. Thus, such a transition is ignored in the model. An explanation of the singlet-versus-triplet designation for states is given as Figure 2-5.

Radiative transitions $S_0 \rightarrow S_{n>1}$ are possible, but they can be ignored in the model because internal conversion (i.e., non-radiative intrasystem transition) and vibrational relaxation from singlet states $S_{n>1}$ to S_1 is fast relative to other transitions from these higher states; this is known as Kasha's Rule [7]. However, internal conversion from S_1 to S_0 is *not* efficient because in general $\Delta E_{S_1 \rightarrow S_0} \gg \Delta E_{S_n \rightarrow S_m}$, where $n = m + 1$ and $m \geq 1$. The effect of state energy difference on internal conversion efficiency is visualized in Figure 2-6.

The rate equations for the system of Figure 2-3 are

$$\frac{\partial}{\partial t}N_0 = -k_{abs}N_0 + k_{vib}N_1 \tag{2.1}$$

$$\frac{\partial}{\partial t}N_1 = -(k_{vib} + k_{STED})N_1 + (k_{STED} + k_{fluor})N_2 + k_{phos}N_4 \tag{2.2}$$

$$\frac{\partial}{\partial t}N_2 = k_{STED}N_1 - (k_{flour} + k_{STED})N_2 + k_{vib}N_3 - k_{isc}N_4 \tag{2.3}$$

$$\frac{\partial}{\partial t}N_3 = k_{abs}N_0 - k_{vib}N_3 \tag{2.4}$$

$$\frac{\partial}{\partial t}N_4 = k_{isc}N_2 - k_{rxn}N_4 \tag{2.5}$$

where N_i is the population in energy level E_i (let E_4 be the triplet energy level) and stimulated emission at $\omega = (E_2 - E_1)/\hbar$ with rate constant k_{STED} has been introduced. For efficient STED, one wants $k_{STED} \gg k_{fluor}$, $k_{STED} \gg k_{isc}$, and $k_{STED} \ll k_{vib}$. Thus, the duration $1/k_{STED}$ of the STED pulse should be much longer than the mean vibrational relaxation time in the singlet manifolds, yet also much shorter than both the fluorescence lifetime and the mean time to intersystem crossing from E_2. Also, the temporal spacing between excitation and STED pulses should be longer than $1/k_{vib}$ but much shorter than either $1/k_{fluor}$ or $1/k_{isc}$. Finally, the duration $1/k_{abs}$ of the excitation pulse should be much shorter than either $1/k_{fluor}$ or $1/k_{isc}$. The significance of this multitude of constraints lies in the proper matching of candidate resist kinetics to suitable optical systems, as discussed in Section 3.2.

2.3.2 Review of Contributions to Resolution Enhancement in Microscopy

Stimulated emission depletion has enabled $\Delta x = 16$nm lateral resolution and $\Delta z = 33$ to 60nm vertical resolution of fluorophores in so-called 4Pi confocal microscopy systems with NA = 1.4 immersion lenses [8]. Because fluorophores often serve to track biological molecules with which they naturally or by design interact with specifically, STED microscopy has enabled imaging of biological systems with remarkable resolution. Some fluorophores have no significant intersystem crossing rate; in this

case, continuous-wave illumination is possible and has been demonstrated [9]. Usually, though, ultrafast (subnanosecond) pulsing and synchronization is required for effective STED, limiting the technique's widespread adoption in the life sciences.

Chapter 3

Considerations for a Nodal Lithography System

Metastable atom localization, photochromic layer aperturing, and quantum state quenching via STED have all used far-field optical nodes to increase resolution; only metastable atom localization and photochromic layer aperturing have been demonstrated for lithography. Direct patterning of a resist via STED can increase resolution and decrease cost in both low-volume research and high-volume manufacturing. To accomplish this, three things must be considered:

- Resist formulation depends on the applicability of existing resist systems,
- optical pulse width is bounded by resist kinetics, and
- the choice of patterning scheme is determined by throughput requirements.

3.1 Resist Formulation Depends on Applicability of Existing Systems

Whereas the STED photophysical transition competes mainly with that of fluorescence in a photoactive compound used for microscopy, in a lithography application

the STED transition competes mainly with that of intersystem crossing. Depending on transition kinetics and on photoreversibility, one may

1. use an existing (i.e., commercially available) resist,
2. sensitize an existing resist,
3. insert a photoactive compound (PAC) into a known resin system, or
4. synthesize a designed PAC/resin system.

The options are in order of increasing difficulty.

3.1.1 Existing Resists

The applicability of an existing resist to stimulated emission depletion depends on the photophysical transition kinetics of the photoactive compound (PAC) or alternatively on the photoreversibility of the final product. Chemical change generally occurs from a triplet state because electron orbitals of the same spin cannot resonate in and out of an overlapping spatial distribution; chemical dissociation is thus more favorable than if the electrons are of opposite spin. Because commercial photoresists are designed for high quantum yield, their PACs are selected for high intersystem crossing rates that STED might not be able to outcompete – if $1/k_{isc} \sim 10$ps and $1/k_{vib} \sim 1$ps, there's not much room for efficient STED.

Existing resists are generally optimized for exposure at a particular wavelength band, but photoreversal to the initial (unexposed) state may be possible using a different wavelength band. Unfortunately, relevant kinetic data are sparse in the academic and patent literature because such data are not of interest to achieving good results in the forward direction, which is the direction usually focused on. Also, chemical structure information, via which relevant reversal kinetics may be theorized, is sparse as well – particularly for modern submicron resists – due to competition in industry. One example of a photoreversible resist is poly(vinyl cinnamylidene acetate), a negative resist introduced in 1966, in which bonds form between functional groups on different polymer backbones using the 365nm Mercury line and can be broken

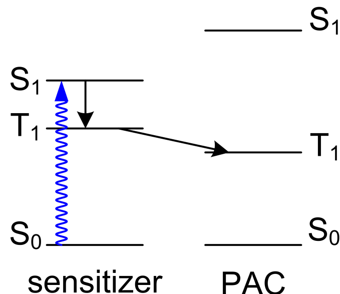

Figure 3-1: Energy level diagram for triplet sensitization. The sensitizer's S_1 level lies below that of the PAC; thus, a longer wavelength may be used for illumination. Singlet energy transfer is endothermic and thus unfavorable. Triplet energy transfer may occur if the sensitizer's T_1 level is *above* that of the PAC.

using the 254nm Mercury line [10]. However, poly(vinyl cinnamate), which is simply poly(vinyl cinnamylidene acetate) with one rather than two ethylenes connecting the monomer unit's phenyl and carbonyl groups, is well known to have poor adhesion to glassy surfaces like oxidized silicon [11]. Further investigation is needed to determine whether use of a modern adhesion promoter such as hexamethyldisilazane (HMDS) could resolve this concern.

3.1.2 Sensitization of Existing Resists

Another option toward a STED-receptive resist is the sensitization of an existing resist at a wavelength outside its normal absorption band. Sensitization is the use of a molecule that absorbs at the illumination wavelength and that transfers either energy or an electron to another molecule that does not absorb at the illumination wavelength; this second molecule (for example, the existing resist PAC) then does productive chemistry. This approach leaves intact pre-optimized (by the manufacturer) kinetic relationships among the existing PAC, resin, and various additives. For example, the dye 2-ethyl-9,10-dimethoxyanthracene may be added to a commercial 193nm photoresist (JSR AR1863J) to make the resist sensitive to 400nm light [4].

Sensitization works either by *energy transfer* or by *electron transfer* from the sensitizer to the normal photoactive compound. Sensitization by energy transfer

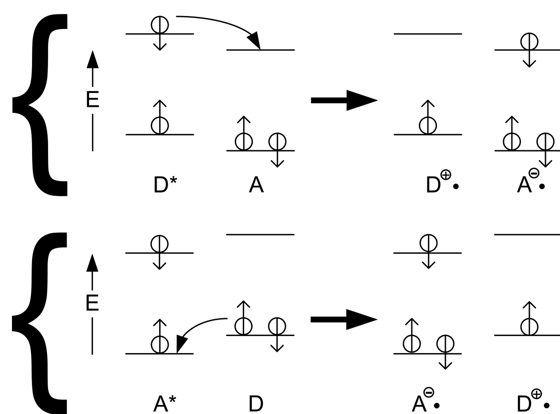

Figure 3-2: *Photoinduced Electron Transfer.* Both top and bottom diagrams show electron transfer from a donor D to an acceptor A, after which the donor is a positively-charged radical and the acceptor is a negatively-charged radical. In the top diagram, the donor is excited and transfers its high-energy electron to the acceptor's lowest unoccupied molecular orbital. In the bottom diagram, the acceptor is excited, which leaves an electron vacancy in the lower state; the donor sees this lower-energy vacancy and transfers an electron.

requires the sensitizer to get to its excited triplet state (see Figure 3-1); thus, triplet sensitizers typically have high intersystem crossing rates ($\sim$ 10ps) that may challenge STED. Photoinduced electron transfer is depicted in Figure 3-2. Both top and bottom diagrams show electron transfer from a donor D to an acceptor A, after which the donor is a positively-charged radical and the acceptor is a negatively-charged radical. In the top diagram, the donor is excited and transfers its high-energy electron to the acceptor's lowest unoccupied molecular orbital. In the bottom diagram, the acceptor is excited, which leaves an electron vacancy in the lower state; the donor sees this lower-energy vacancy and transfers an electron [6].

One can use a compound D with efficient intersystem crossing to produce the triplet state of another compound A through electron exchange energy transfer. If the highest occupied molecular orbital of A is *above* that of D's ground state, and if the lowest unoccupied molecular orbital of A is *below* that of D's ground state, then one gets an addition of the two processes depicted in figure 3-2. That is, an electron exchange has occurred such that $D^* \rightarrow D$ and $A \rightarrow A^*$. The electron exchange

transfer rate k_{ee} is given by

$$k_{ee} = KJe^{-2r_{DA}/L} \ ,$$

where r_{AD} is the distance between D and A, L is the sum of van der Waals radii, K is related to the magnitude of specific orbital interaction that promotes electron exchange, and J is a spectral overlap integral that describes the extent to which the absorption spectrum of D overlaps that of A, normalized for the extinction coefficient ϵ_A of A [6]. If D's $k_{isc} < k_{ee}$ and if intersystem crossing is efficient in A, one can still use D to achieve the excited triplet state of A; for externally induced processes like stimulated emission depletion to compete, intersystem crossing in D must be relatively inefficient.

3.1.3 Modular Approach: PAC Insertion Into Known Resin Systems

One may instead insert a special, STED-friendly PAC into a known resin system. The PAC should have a low intersystem crossing rate k_{isc} to allow for $k_{STED} \gg k_{isc}$, but not so low as to require a burdensome resist-exposure time[1]. One difficulty here is that obtaining an existing resist system without its PAC would require an accommodating resist manufacturer; the competitive nature of the resist industry may preclude such a gift. Also, even if a high-performance resin system could be obtained without its normal PAC, the new PAC may upset resist properties in ways that could not be easily troubleshooted due to the proprietary nature of the resin system formulation.

3.1.4 Synthesis of Designed PAC/resin System

What follows is an introduction to the considerations involved in the design of a nodal negative photoresist. Only the design of the PAC in this case is constrained by the STED approach.

[1]obviously, this exposure time requirement is less crucial in low-throughput applications

Design of the PAC Much of photochemistry is an exercise in controlling relative rates. The quantum yield Φ_n of a process n can be defined as $\Phi_n = \frac{k_n}{\sum_i k_i}$, where k_n is process n's rate constant and the variable i enumerates over all possible processes from the excited state [6]. Alternatively, $\Phi_n = \frac{\text{\# of molecules that undergo process } n}{\text{total \# of photons absorbed}}$. Fluorescence lifetimes for most organic structures are typically $\sim 100\mu$s to 1ns. The longer lived an excited state, the better chance it has to do productive photochemistry. For example, the intersystem crossing rate in benzophenone is $\sim 10^{11}\, s^{-1}$, meaning its photochemical activity is dominated by triplet states.

There are various pathways for unproductive quenching of excited states. In the design of fluorescent compounds, there is the "free rotor" or "loose bolt" effect: as substituents with many degrees of vibrational/rotational degrees of freedom are added to a molecule, the process of internal conversion becomes more efficient. This decreases fluorescence quantum yield. There is also quenching through collision with another molecule. Given a unimolecular excited state decay-rate constant $k_f = k_{fluor}$ (assuming the excited state lifetime is comparable to the fluorescence lifetime), a bimolecular diffusion rate constant k_{diff}, and a concentration of colliding molecule $[x]$, $k_f \lesssim k_{diff}[x]$ is a competitive scenario. Typically, $k_f \sim 10^5 - 10^8 s^{-1}, k_{diff} \sim 10^{10} M^{-1} s^{-1} \Rightarrow [x] \sim 10^{-5} - 10^{-2} M$. More generally, consider the pathways

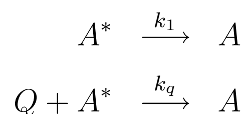

$$\begin{aligned} A^* &\xrightarrow{k_1} A \\ Q + A^* &\xrightarrow{k_q} A \end{aligned}$$

where the lifetime of the excited state of species A, denoted by A^*, without the quencher species, Q, is $\tau_1 = 1/k_1$; and the lifetime of A^* with Q present is τ_2. Then $1/\tau_2 = k_1 + k_q[Q] = 1/\tau_1 + k_q[Q]$. This type of analysis is termed Stern-Volmer analysis [6].

Choice of Resin There are five conditions for a resin. First, it need not be photosensitive, but it must be capable of insolubilization via reaction with the activated sensitizer molecule. Second, prior to exposure, it must be soluble in a solvent system.

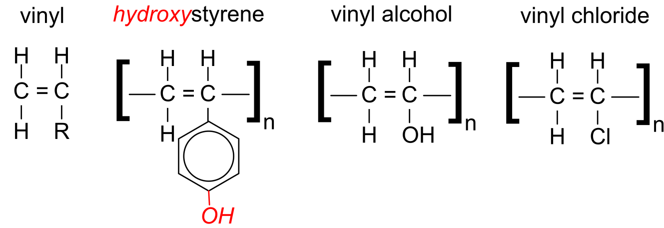

Figure 3-3: *Examples of Vinyl Polymers.* The vinyl monomer is at left. The “R” is a placeholder. Common examples of vinyl polymers include poly(vinyl benzene), which is also called poly(styrene) or just styrene; poly(vinyl alcohol); and poly(vinyl chloride). The brackets and the “n” indicate that a linear polymer is a repetitive chain of monomer units. With a hydroxyl group attached to the other side of the benzene ring in styrene, the polymer becomes poly(hydroxystyrene), or PHOST; derivatives of PHOST are used in commercial 248nm resists.

Third, it must be capable of wetting and adhering to a variety of surfaces. Fourth, upon air evaporation, the resin must form a uniform film but not lose its solubility in its solvent. Fifth, the processed resin image must be resistant to aqueous solutions [12].

Resins typically possess *chemical unsaturation*, meaning they feature a chemical bond between two carbon atoms through two shared electron pairs. Upon activation, one electron pair can be shared by carbon atoms of adjacent polymer molecules that are similarly unsaturated. This sharing is termed *cross linking*, and it increases the hardness, the chemical resistance, and the adhesion to the substrate. Examples of linear polymer resins, which contain a basic backbone structure that may have various functional groups connected, are poly(styrene), poly(vinyl alcohol), and poly(vinyl chloride) (see Figure 3-3). With a hydroxyl group attached to the other side of the benzene ring in styrene, the polymer becomes poly(hydroxystyrene), or PHOST; derivatives of PHOST are used in commercial 248nm resists.

3.2 Optical Pulse Width Bounded By Resist Kinetics

The illumination scheme used for nodal photolithography depends on the kinetics of the resist. If the photoactive compound has an intersystem crossing rate $k_{isc} \gtrsim 1/(100\text{ps})$, the most suitable scheme is likely a Ti:Sapphire system with a pulse stretcher for STED pulses. If the intersystem crossing rate $k_{isc} \lesssim 1\ \text{ns}^{-1}$, a diode system with synchronization electronics is appropriate. If the resist is photoreversible, continuous-wave sources are suitable.

3.2.1 Ti:Sapphire System with Pulse Stretching for Fast Kinetics

If the photoactive compound (PAC) has an intersystem crossing rate $k_{isc} \gtrsim 1/(100\text{ps})$, then the sum of the excitation pulse width, interpulse separation, and depletion pulse width should be much less than 100ps for the STED process to be efficient. Commercial ($\sim$ \$100k) Ti:Sapphire lasers are suitable for this. They can generate $\sim$ 200fs pulses tunable in the visible and near infrared, and with the help of a beta barium borate (BBO) crystal can also produce synchronized pulses at double the frequency of the fundamental – this process is called second harmonic generation (SHG).

Dispersive pulse broadening with gratings can stretch the fundamental out to tens of picoseconds; in fact, this technique is the basis for the chirped pulse amplification (CPA) technique that makes high-power ultra-short-pulse lasers like the Ti:Sapph feasible [13]. Since timing between the doubled (used for excitation) and fundamental (used for STED) pulses can be controlled to picosecond precision with an optical delay stage, this is a recipe for successful STED in high-k_{isc} PACs and has been demonstrated in STED microscopy for fluorophores of $k_{fluor} \sim 1\ \text{ns}^{-1}$ [14]. To tune the wavelength separation of excitation and STED pulses, an optical parametric oscillator (OPO) can be used in conjunction with the frequency-doubling crystal [15].

3.2.2 Diode System for Not-as-Fast Kinetics

If the intersystem crossing rate $k_{isc} \lesssim 1\ \text{ns}^{-1}$, a diode system with synchronization electronics is appropriate. Commercial (∼ $20k) diode systems are available that drive multiple (∼ 100ps)-pulse-width laser diodes with picosecond-precision synchronization [16]. Depending on how small k_{isc} is, nanosecond lasers or even pulsed LEDs may be used, greatly reducing the cost of optics.

3.2.3 CW Sources for Photoreversible Resists

If the dissolution inhibition (negative resist) or dissolution enhancement (positive resist) property of exposed photoresist is photoreversible, continuous-wave illumination sources are suitable. The example of adhesion-poor poly(vinyl cinnamylidene acetate), which fits this description, was discussed in Section 3.1.1. A photochromic material, such as that used in absorbance modulation optical lithography (see Section 2.2), that exhibits a sharp difference in dissolution rate between the two photoisomeric states may enable CW nodal lithography.

3.3 Patterning Scheme Determined by Throughput Requirements

Mask-less direct writing for low-volume research and double exposure interference lithography with trim masks for high-volume manufacturing can cut costs for far-field photolithography through eliminating the need for precision mask generation and alignment. The salient features of such techniques as they apply to nodal photolithography will now be discussed.

3.3.1 Serial Direct-Write for Low Throughput

One may envision a serial direct-write scheme as in Figure 3-4. The substrate may be scanned relative to the beam given a pulse repetition rate much larger than the stage

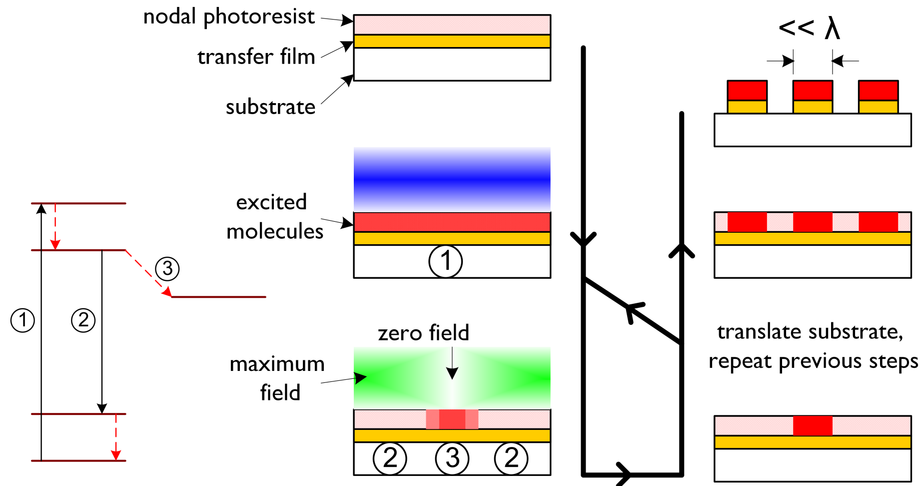

Figure 3-4: The energy level diagram at left enumerates the (1) absorption, (2) emission, and (3) intersystem crossing transitions. First, an excitation pulse brings a focal spot of photoresist to the excited state manifold. Next, a depletion pulse, patterned with a node in its center of focus, brings all of the excited resist except for that in the nodal region to the ground state. Then, intersystem crossing enables chemical change in the nodal region. Finally, the stage is stepped or scanned to repeat the process and generate an arbitrary pattern for subsequent development and etching.

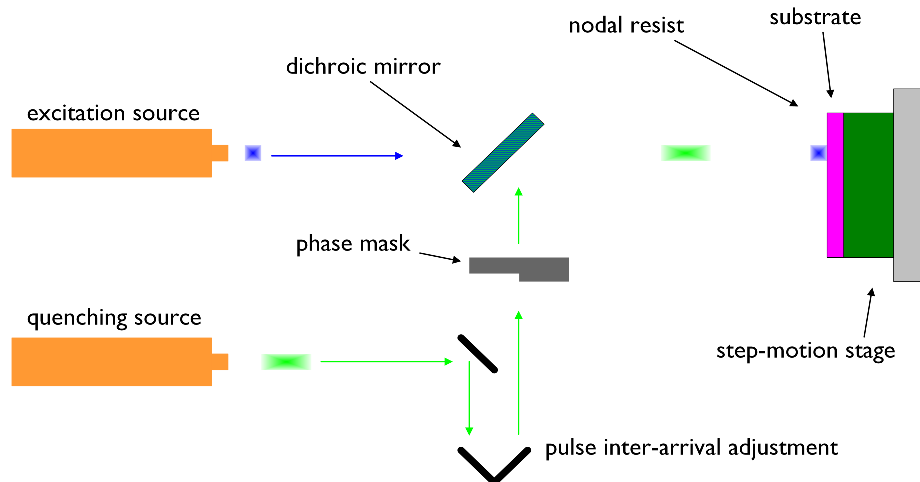

Figure 3-5: A potential nodal lithography system. A lens for focusing to the substrate is pictorially omitted to reduce clutter. If the excitation and quenching sources are diodes, driver electronics can control synchronization and thus a delay stage is unnecessary. If a Ti:Sapphire system is used, the excitation and quenching pulses come from the same source (see Section 3.2.1).

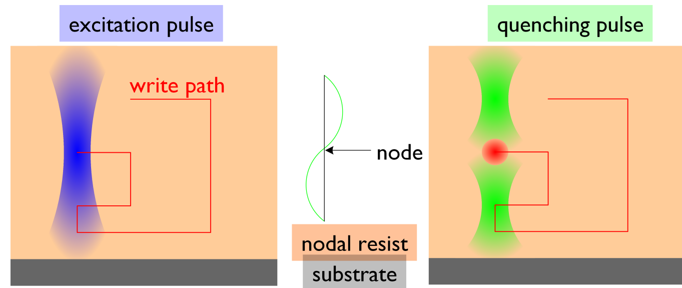

Figure 3-6: Two quenching pulses that (1) are coaxial with the excitation pulse, (2) have foci that are respectively shallower and deeper than the focus of the excitation pulse, and (3) are out of phase by p, can quench all molecules with the exception of those near the excitation beams focus. This operation leaves a single excited 3-D spot, resulting in selective exposure at that location.

scanning rate. Alternatively, a step-and-repeat scheme would create a dot matrix pattern. A possible optical system for this scheme is depicted in Figure 3-5. Stage stepping perpendicular to the substrate, along with upstream light modulation along that axis, would enable three-dimensional patterning (see Figure 3-6).

3.3.2 Double Exposure Interference Lithography for High Throughput

One way to achieve high-throughput nodal photolithography would be to combine interference lithography with low-precision mask trimming in a double exposure scheme [17]. Using an achromatic dual grating pair to achieve a small-linewidth interference pattern via STED, the substrate would then be stepped and re-exposed to achieve a spatial frequency beyond the diffraction limit. A low-precision mask under traditional one-wavelength exposure would then trim the interference pattern to define the components along one axis of the desired final 2D pattern. After development and etching, the interference exposure and trimming process is repeated for the final 2D pattern components along the orthogonal axis. Although two resist cycles for each layer seems expensive, double patterning – independent of STED – is the front-runner technique under development for getting photolithography to the 22nm node and beyond [2].

Chapter 4

Experimental Realization of STED

The first step toward a working nodal lithography system is verification of stimulated emission depletion. This requires generation and synchronization of excitation pulses and STED pulses, choice of a material under test for which verification of STED can be performed rapidly, appropriate positioning and focusing of the pulses, and a mechanism for rapid verification of STED. A way to stretch the STED pulse in time may also be desired. Once the STED effect is verified, one may swap in various resist candidates and implement a patterning scheme.

4.1 Generate and Synchronize Excitation Pulses and STED Pulses

In earlier work, a Ti:sapphire laser was effective for STED [14]. Its high CW output power ($\sim$ 1 Watt) helps to achieve high I_{max}/I_{sat} (see section 1.2), and its routine incorporation with nonlinear crystals for second harmonic generation produces synchronized pulses at half the wavelength of the fundamental; these doubled-frequency pulses have been used successfully for excitation while the fundamental-frequency pulses were used for STED [14]. The system I used (see Figure 4-1) comprises

- a c.w. argon ion pump laser, which couples into the cavity via a dichroic mirror
- a birefringent filter to select the central wavelength of the oscillation

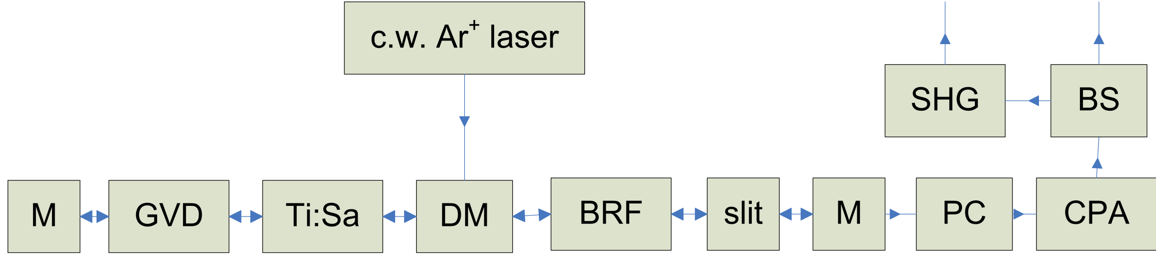

Figure 4-1: A simplified block diagram of the system used to generate synchronous excitation and STED pulses. A continuous-wave argon ion pump laser couples into the cavity via a dichroic mirror (DM). Along the left "leg" is a Ti:sapphire crystal, a prism system for correcting group velocity dispersion (GVD), and a cavity end mirror (M). Along the right "leg" is a birefringent crystal (BRF), slit, output mirror (M), Pockels cell (PC), chirped pulse amplification system (CPA), beamsplitter (BS), and second harmonic generator (SHG).

- the Ti:sapphire gain medium, which provides self-mode-locking with the aid of a slit
- prisms for correcting group velocity dispersion
- a Pockels cell for pulse picking
- chirped pulse amplification for increased output power
- and second harmonic generation for creating the STED pulse.

What follows in this section are paragraphical expansions of the latter five items.

4.1.1 Self-mode-locking in a Ti:sapphire System

Titanium-doped sapphire is a material with a significant third-order susceptibility term in the Taylor expansion of its macroscopic polarization as a function of incident electric field. What this means is that, under intense radiation, Ti:sapphire has a nonlinear index of refraction that looks like

$$n(r) = n_0 + n_2 I(r) \ ,$$

where r is the transverse radial coordinate and I is the intensity of a (Gaussian) beam traveling through the material. Since the optical path length is $p(r) = n(r) \cdot d$, where

d is a constant thickness, by setting n to be constant and d to vary with r, one can visualize a focusing "lens" when $n_2 > 0$. Use of a slit in the cavity preserves intensity maxima, which are focused, while accelerating the loss of low intensities, which do not experience a Kerr lens. This provides mode locking akin to that of systems with saturable absorbers for passive mode locking [18].

4.1.2 Correcting Group Velocity Dispersion (GVD)

A short optical pulse necessarily has a wide spectral width. This makes it vulnerable to dispersion. The time-domain representation of a pulse's electric field while propagating through a transparent medium looks like

$$E(t,x) \propto \exp\left(i\omega_0(t - \frac{x}{v_\phi(\omega_0)})\right) \times \exp\left(-\Gamma(v_g,x)(t - \frac{x}{v_g(\omega_0)})^2\right) \ ,$$

which is to say that the phase velocity v_ϕ is of no concern because it is in the phase term, which has no observable consequence. Not only does the group velocity v_g delay the pulse, but through the form factor Γ it broadens the pulse envelope. A pair of prisms is used to correct for GVD by introducing "negative" dispersion, meaning high frequencies are directed through a shorter optical path length than low frequencies; in the Ti:sapphire, the pulses experience positive dispersion [18].

4.1.3 Pulse Picking with a Pockels Cell

A Pockels cell is a serial cascade of an electro-optic modulation crystal and a polarizer. The electro-optic crystal has ordinary and extraordinary crystal axes, and light polarized along one axis will experience a different index of refraction than along the other. The difference in indices is controllable by an external voltage. This property allows an electrical signal to rotate the linear polarization of a pulse traveling through the material by 90° such that it either passes through or is blocked by the subsequent polarizer. The modulation can be done quickly enough to turn a 76MHz train of pulses into a 1kHz train, which is the repetition rate in my setup.

4.1.4 Chirped Pulse Amplification (CPA)

A chirped pulse is one for which high frequency components are temporally retarded (positive chirp, or up-chirp) or advanced (negative chirp, or down-chirp) relative to low frequency components. Chirping a previously unchirped pulse will temporally broaden it. Chirped pulse amplification is necessary because the amplification of ultrashort pulses can generate intensities above the damage threshold of an optical amplifier. A pulse is sent through a grating pair to up-chirp it [13]. After that, it is sent through a multipass or regenerative amplifier. Whereas a multipass amplifier relies on an assembly of mirrors for a given number of passes through the amplifying medium, a regenerative amplifier uses a Pockels cell for entry to and exit from the resonator; my setup uses a regenerative amplifier with Ti:sapphire as the gain medium. After amplification, the pulse is down-chirped by another grating pair, returning the pulse to its original temporal width.

4.1.5 Second Harmonic Generation (SHG)

For two pulses at frequencies ω_1 and ω_2 to produce a third at higher frequency ω_3, both energy and momentum must be conserved. Thus,

$$\begin{aligned} \omega_1 + \omega_2 &= \omega_3 \\ k_1 + k_2 &= k_3 \end{aligned}$$

must be satisfied. When all pulses are co-linear, the second relation (the phase-matching condition) becomes

$$\frac{n_1}{\lambda_1} + \frac{n_2}{\lambda_2} = \frac{n_3}{\lambda_3} ,$$

which cannot be satisfied in a normal material in which the index of refraction varies as $1/\lambda$. With a birefringent material, however, by adjusting the angle between its optical axis and the direction of pulse propagation, the pulses – at different polarizations – may satisfy the phase-matching condition for a selected wavelength. In my setup, the crystal is β-barium borate (BBO), and $\omega_1 = \omega_2 = 810$nm. This produces $\omega_3 = 405$nm

light with typically tens of percent conversion efficiency [18].

4.2 Choose a Material Under Test for Concurrent Verification

The material under test should be chosen so as to reduce the time necessary for processing whether or not STED has been effective for it. Thus, I did not use a photoresist-like material; this would have required a time-consuming chemical development step between exposure and verification. In addition, it would be difficult to decouple the susceptibility of the photoresist material to STED and the integrity of the optical setup. This deemed wise the choice to use a styryl dye, as these have historically performed well in STED microscopy work [19]. To enable easy verification of STED with a streak camera (see section 4.4), the dye must have a high fluorescence yield, it must be photostable, and it must have a large cross-section for stimulated emission at the 810nm wavelength of the STED pulse.

4.2.1 High Fluorescence Yield

High fluorescence yield means that the rate constant k_{fluor} for fluorescence must be much higher than the rate constants of competing processes from the excited singlet state such as internal conversion and intersystem crossing. In considering laser dyes, i.e. dyes that have documented use as laser gain media, high fluorescence yield may be assumed. This is because the electronic transition corresponding to *spontaneous* fluorescence is identical to that of stimulated emission, and stimulated emission is an *induced* transition that, in laser dyes, is able to outcompete the same processes that fluorescence must. High fluorescence yield enables high contrast differentiation (if the STED process works) between the presence and absence of a STED pulse following an excitation pulse, particularly because any optical detector has a noise floor.

4.2.2 Photostability

Photostability means that the material is able to undergo numerous cycles of excitation and de-excitation (either spontaneously or via stimulated emission) without "bleaching", numerous in the sense that the streak camera will integrate the results of several cycles for high signal-to-noise, and so, for example, integration for one minute at a 1kHz repetition rate means 6×10^4 cycles. In a lithography (or imaging) context, the photostability requirement is reduced because pixel dwell time will not be considerably longer than 1ms, and even the proximity effect due to high-density beam scanning will not re-excite a given focal volume more than a few tens or hundreds of times. Photobleaching is characterized by irreversible chemical change, and its probability increases with radiation intensity, meaning that STED pulse intensity cannot be raised arbitrarily high in the hope of achieving higher I_{max}/I_{sat} without detrimental side effects.

4.2.3 Large Cross-section for Stimulated Emission

$I_{sat} = \frac{1}{\sigma\tau}$, where σ is the cross-section for stimulated emission in the material under test and τ is the temporal width of the STED pulse. Because I_{sat} should be minimized for efficient STED, the material under test should be chosen so that its σ is as large as possible for the wavelength $\lambda = 810$nm of the STED pulse. Styryl 9M has strong performance as a gain dye in the wavelength range $780-860$nm [18], so it was chosen for my experiment. Pyridine 2 was used successfully in prior work [14], but its optimal range of operation is $690 - 770$nm (the prior work tuned its Ti:sapphire laser to emit in this range).

4.3 Position and Focus Pulses Appropriately

To quench the fluorescence of the Styryl 9M dye, the focal volume of the STED pulse must encompass that of the excitation pulse. Since both pulses are Gaussian transverse modes (TEM_{00}), the STED pulse focal volume must be larger than that of

the excitation pulse; otherwise, the outer perimeter of excitation might not experience a STED intensity large enough to quench fluorescence there. Also, a too-tight STED pulse focus could cause continuum (white light) generation in the dye, which could re-excite depleted molecules.

However, the STED pulse must be focused tightly enough for high I_{max}/I_{sat}. In my setup, CW power for the $\lambda = 810$nm light can be tuned to ~ 40mW, repetition rate is 1kHz, pulse duration is $\tau \sim 200$fs, and I will assume that the stimulated emission cross section $\sigma \sim 10^{-16}\text{cm}^2$. Using these numbers, with a pulse diameter of ~ 0.5cm,

$$\begin{aligned}
\text{pulse energy} &\approx \frac{40\text{mW}}{1\text{kHz}} = 40\mu\text{J} \\
\Rightarrow \text{irradiance} &\approx \frac{40\mu\text{J}}{0.25\text{cm}^2} = 160\frac{\mu\text{J}}{\text{cm}^2} \\
\Rightarrow \text{intensity } (I_{max}) &\approx \frac{160\mu\text{J/cm}^2}{200\text{fs}} = 800\frac{\text{MW}}{\text{cm}^2} \cdot \frac{1 \text{ photon}}{hc/\lambda \text{ Joules}} \approx 3 \times 10^{27}\, \frac{\text{photons}}{\text{cm}^2 \cdot \text{s}}
\end{aligned}$$

Since $I_{SAT} \equiv \frac{1}{\sigma\tau} \approx 5 \times 10^{28}\ \frac{\text{photons}}{\text{cm}^2 \cdot \text{s}}$, $I_{max}/I_{sat} \sim 10^{-1}$. Since $I_{max} \gg I_{sat}$ is optimal for STED, focusing is necessary. A focal diameter of even 500μm will ensure that $I_{max} > I_{sat}$; although STED might not be efficient in that case, it should be observable.

4.3.1 Excitation Volume Enclosed by STED Volume

Figure 4-2 depicts the STED verification system as a whole, and highlights the importance of appropriate beam deflection and focusing so that the excitation volume is enclosed by a STED volume that is small enough to achieve sufficient fluence, yet large enough to avoid white-light generation (see section 4.3.2). Beams were overlapped and focused by (laser-goggle protected) eye onto a slip of paper positioned to correspond to the front surface of the sample cuvette. This is because of the intuitive Beer-Lambert law for absorption,

$$n(z) = n_0 \text{e}^{-\alpha z} \ ,$$

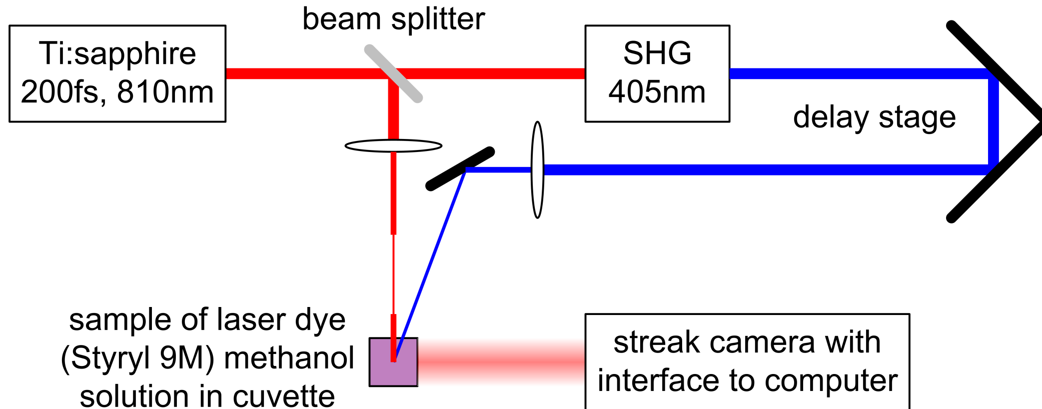

Figure 4-2: A simplified diagram of the integrated system for STED verification, highlighting the importance of appropriate beam deflection and focusing. SHG: Second harmonic generation. In the actual system, both beams are steerable by micro-screw mirror mounts, and both focusing lenses have a 100cm focal length. The focal volume of the STED beam is not placed inside the sample because continuum generation in the sample must be avoided. The streak camera is oriented so that it only collects radiation emitted by the sample.

where $n(z)$ is the number of photons retrieved from an absorbing medium along z, n_0 is the number of photons impinging on it, and $\alpha > 0$ is the linear absorption coefficient. For this same reason, the pulse action volume was also placed close to the cuvette surface facing the streak camera.

4.3.2 Too-Tight STED Pulse Focus Causes Continuum Generation

Placing a material such as a paper card at the focus of the STED beam produces white light and a high-pitched "burning" sound. Continuum generation with high-peak-power light pulses is governed by self-phase-modulation, i.e. the Kerr effect that the Ti:sapphire uses productively for self-mode-locking. To avoid continuum generation in the context of STED and for a given continuous-wave power and pulse repetition rate, one must either stretch the STED pulse or focus the pulse outside the sample (i.e., in the air). I chose to focus the pulse outside the sample rather than stretch the pulse (see section 4.5 for my reasoning).

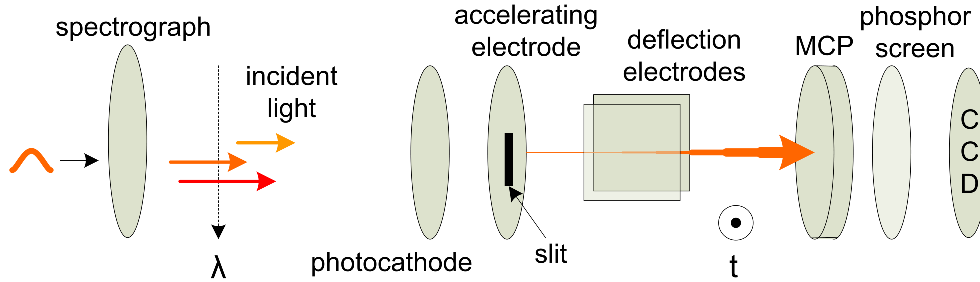

Figure 4-3: Illustrated are the elements of a streak camera. The spectrograph spatially separates frequency components. The photocathode converts photons to electrons. The accelerating electrode directs electrons representing a certain wavelength band through a slit to the deflection area, where electrodes controlled by a triggered sweep voltage generator form a streak in time on the microchannel plate (MCP). The MCP acts as an electron multiplier tube, spitting its amplified electron signal onto the phosphor screen, which is recorded by a CCD camera, which is interfaced to a computer.

4.4 Track Pulse Spacing and Verify STED with a Streak Camera

A streak camera is essentially a serial cascade of a spectrograph (Chromex 250is), a photo-cathode ray tube, and a fiber-coupled CCD camera (see Figure 4-3). In addition, the photo-CRT has an electron multiplier tube ("microchannel plate") for internal amplification. The post-spectrograph apparatus (Hamamatsu Streakscope C4334) claims a temporal resolution of $\lesssim$ 15ps and a trigger jitter of $\lesssim$ 20ps. Using the streak camera, one can track interpulse spacing for optical delay guidance. Also, the direct verification of STED is performed with the streak camera.

4.4.1 Tracking of Interpulse Spacing for Delay Guidance

The delay stage depicted in Figure 4-2, a retroreflector mounted on a computer-controlled linear track, has precision approaching a few picoseconds, i.e. better than the $\lesssim$ 15ps temporal resolution of the streak camera. The optimal separation between excitation and STED pulses is likely less than 15ps [19], so this presents a problem. The method used for establishing approximate interpulse spacing is as follows:

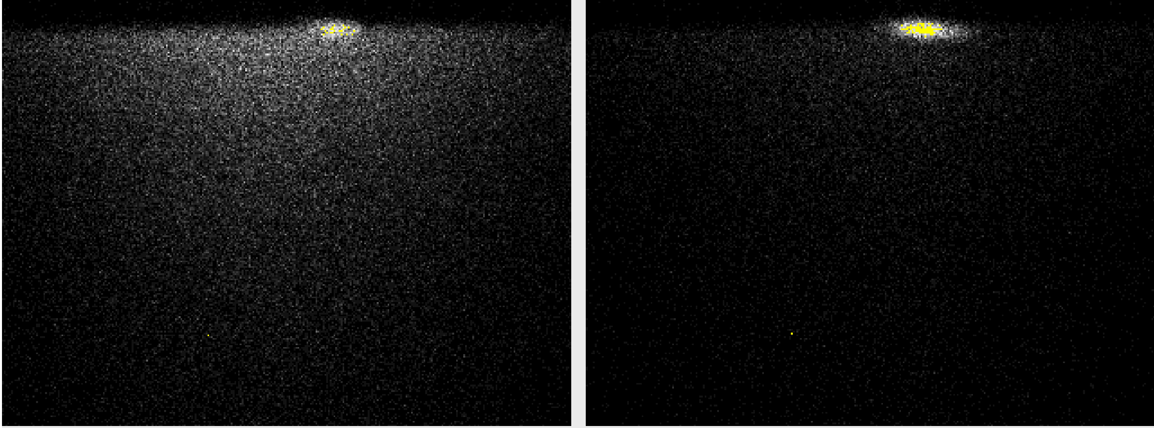

Figure 4-4: At left is a $\sim$ 5-minute integration time streak image for only the 405nm excitation pulse incident on the Styryl 9M sample. The horizontal range is $\sim$ 140nm, centered at 800nm. The vertical range is $\sim$ 1ns, triggered on the arrival of the 405nm pulse. At right is an image for the 405nm excitation pulse followed $\sim$ 10ps later by the 810nm STED pulse, with all other parameters being the same.

1. Triggering the streak camera on the periodic arrival of one of the pulses.

2. Scan the delay stage until the other pulse appears in the real-time streak camera output.

3. Measure the approximate interpulse spacing on the computer, recognizing the $\lesssim$ 20ps timing jitter.

4. Drive the delay stage the number of "steps" corresponding to the time interval needed to close the gap.

This method is carried out using scattered light, i.e. a scattering element (e.g. tissue paper) is placed in the sample cuvette holder for the duration of the calibration.

4.4.2 Verification of STED

The initially-promising results of a long-integration-time experiment are given as Figure 4-4. The integration time is 12×10^3 "counts" as determined by the acquisition software, which corresponded to $\sim$ 5 minutes of real time. The streak image on the left, for only the 405nm excitation pulse incident on the Styryl 9M sample, shows bright spots that indicate photon hits. The streak image on the right, for the 405nm

excitation pulse followed $\sim$ 10ps later by the 810nm STED pulse (with all other parameters being the same), shows a noticeable reduction in hits for this spectral-temporal window.

However, a third long-integration-time experiment, a confirmation of the 405nm-only situation, yielded a streak image that looks like the one on the right-hand side of Figure 4-4. The presumed explanation for this "time-out" of the dye is photo-bleaching (see section 4.2.2), particularly because real-time "hand-waving" was successful prior to initiation of the long-integration-time trials. Specifically, waving my hand discretely in and out of the path of the unfocused STED beam (without touching the excitation beam) produced significant variation in the real-time fluence of photon hits viewable on the computer monitor interfaced to the streak camera; blocking the STED beam resulted in a sustained surge of hits that vanished when the beam was unblocked, and this effect was easily repeated several times before I decided to commence a long-integration-time trial for posterity.

4.5 Stretch... or Do Not Stretch

According to published simulations, longer pulses ($\tau > 10$ps) not only make STED more efficient (because $I_{sat} = \frac{1}{\sigma\tau}$) but also reduce photo-bleaching (by reducing peak power) [19]. The simulation parameters were $k_{fluor} \sim 1\text{ns}^{-1}$, $k_{vib} \sim 3\text{ps}^{-1}$, $\sigma = 10^{-16}$, and $\lambda_{STED} = 765$nm. These are roughly equivalent to the parameters in my experimental work. Those simulations also showed that, for $\tau = 200$fs, total fluorescence as a function of STED pulse irradiance flattened with increasing irradiance to a quasi-asymptotic value of $\sim 30\%$, meaning that quenching significantly more than two-thirds of excited species is practically impossible given other parameters similar to mine. Two questions arise: (1) Can STED be "good enough" for practical application to lithography with such short STED pulses? (2) What degree of STED pulse stretching can practical lithographic materials accomodate?

4.5.1 STED is Achieved with "Native" Pulse Width

Despite theoretically-predicted low STED efficiency and high photo-bleaching, applications with low pixel dwell time appear feasible with even 200fs pulses. For example, interleaved interference lithography for an enhanced-resolution double-exposure scheme (see section 3.3.2) could be done with only a couple interleave step exposures rather than several, and this could still result in a cost-per-function increase. Because a serial patterning scheme would involve a raster scan of the excitation-and-STED pulse pair, pixel dwell time would be kept at a minimum here as well, and the proximity effect would be reduced somewhat compared to standard laser direct-write methods. Furthermore, the photokinetics of a material that has an irreversible pathway (i.e., a photoresist) may indeed diminish the advantages purported to lie in STED pulse stretching.

4.5.2 Stretching is Advantageous if Allowed by Material Kinetics

STED pulse width is bounded by material kinetics. This idea was explored in section 3.2 for resists, but the idea warrants generalization in order to understand that a certain challenge faces the use of STED in lithography, and that this obstacle is relatively absent when considering the use of STED in imaging. This challenge is that of a *desired* irreversible pathway, for example cross-linking in a negative resist or photo-acid generation in a positive resist. The electronic transition for stimulated emission is the same as that of spontaneous emission, so spontaneous emission (fluorescence) must have some non-negligible rate in order for the stimulated emission cross-section σ to be accessible. The pulse width constraint seems to end here for imaging: it must be smaller than the fluorescence lifetime. Actually, as has been shown [9], molecules with little to no irreversible pathway, or "dark state", can exhibit efficient STED with continuous-wave illumination.

With materials having a desired irreversible pathway (DIP), however, one not only requires a non-negligible rate of fluorescence, but also a superior rate of the

“irreversible” transition (e.g., intersystem crossing for initiation of triplet chemistry). So with a typical fluorescence lifetime of $\sim$ 1ns in organic fluorophores suitable for STED, a suitable intersystem crossing lifetime would be $\sim$ 10 to 100ps, preferably closer to 10ps, for a STED-ready DIP material. Now, the STED pulse must compete kinetically with intersystem crossing, meaning STED pulse width should be $\lesssim$ 10ps. This crosses the theoretical threshold in [19] for low-I_{sat}, photo-bleach resistant STED, in part because the vibrational lifetime in the ground state singlet manifold is often $\gtrsim$ 1ps, and it increases with the degrees-of-freedom complexity of the photolabile material. Because that manifold flushes electrons down to the absolute ground state so that more electrons can be depleted from excited states, the STED pulse should ideally be longer than this vibrational lifetime. It seems that STED lithography faces a “time crunch” uncharacteristic of prior work with STED for imaging; I do hope that a key insight will unlock the path to fruitful further investigation.

Bibliography

[1] Will Conley, Brian Trinque, Daniel Miller, Stefan Caporale, Brian Osborn, Shiro Kumamoto, Matthew Pinnow, Ryan Callahan, Charles Chambers, Guen Su Lee, Paul Zimmerman, and C. Grant Willson. Negative photoresist for 157 nm microlithography: A progress report. In *Advances in Resist Technology and Processing XX*, volume 5039 I, pages 622–626, Santa Clara, CA, United States, Feb 24-26 2003 2003. International SEMATECH, Austin, TX, United States, The International Society for Optical Engineering. Compilation and indexing terms, Copyright 2007 Elsevier Inc. All rights reserved; T3: Proceedings of SPIE - The International Society for Optical Engineering.

[2] B. J. Lin. Optical lithography-present and future challenges. *Academie des Sciences.Comptes Rendus, Physique*, 7(8):858–74, 10 2006. M1: Copyright 2007, The Institution of Engineering and Technology.

[3] K. S. Johnson, J. H. Thywissen, N. H. Dekker, K. K. Berggren, A. P. Chu, R. Younkin, and M. Prentiss. Localization of metastable atom beams with optical standing waves: nanolithography at the heisenberg limit. *Science*, 280(5369):1583–1586, 1998. Compilation and indexing terms, Copyright 2007 Elsevier Inc. All rights reserved.

[4] Hsin-Yu Tsai, Gregory M. Wallraff, and Rajesh Menon. Spatial-frequency multiplication via absorbance modulation. *Applied Physics Letters*, 91(9):094103, 2007. Compilation and indexing terms, Copyright 2007 Elsevier Inc. All rights reserved.

[5] Stefan W. Hell and Jan Wichmann. Breaking the diffraction resolution limit by stimulated emission: stimulated-emission-depletion fluorescence microscopy. *Optics Letters*, 19(11):780–782, 1994. Compilation and indexing terms, Copyright 2007 Elsevier Inc. All rights reserved.

[6] Eric V. Anslyn and Dennis A. Dougherty. *Modern physical organic chemistry.* University Science, Sausalito, Calif., 2006.

[7] Nicholas J. Turro. *Modern molecular photochemistry.* University Science Books, Sausalito, Calif., 1991 (some material cited directly from Columbia University course lectures, from 1999, based on this book).

[8] S. W. Hell. Far-field optical nanoscopy. *Science*, 316(5828):1153–1158, MAY 25 2007. PT: J.

[9] K. I. Willig, B. Harke, R. Medda, and S. W. Hell. Sted microscopy with continuous wave beams. *Nature Methods*, 4(11):915–918, NOV 2007. PT: J.

[10] Arnost Reiser. *Photoreactive polymers : the science and technology of resists.* Wiley, New York, 1989. Arnost Reiser.; "A Wiley-Interscience publication."; Bibliography: Includes bibliographies and index.

[11] C. Grant Willson, Ralph R. Dammel, and Arnost Reiser. Photoresist materials: a historical perspective. In *Optical Microlithography X*, volume 3051, pages 28–41, Santa Clara, CA, USA, Mar 12-14 97 1997. Univ. of Texas/Austin, Austin, TX, USA, Society of Photo-Optical Instrumentation Engineers, Bellingham, WA, USA. Compilation and indexing terms, Copyright 2007 Elsevier Inc. All rights reserved; T3: Proceedings of SPIE - The International Society for Optical Engineering.

[12] William S. DeForest. *Photoresist : materials and processes.* McGraw-Hill, New York, 1975. W. S. DeForest.; Includes bibliographical references and index.

[13] M. Pessot, P. Maine, and G. Mourou. 1000 times expansion/compression of optical pulses for chirped pulse amplification. *Optics Communications*, 62(6):419–421, 6/15 1987.

[14] Thomas A. Klar and Stefan W. Hell. Subdiffraction resolution in far-field fluorescence microscopy. *Optics Letters*, 24(14):954–956, 1999. Compilation and indexing terms, Copyright 2007 Elsevier Inc. All rights reserved.

[15] T. A. Klar, M. Dyba, and S. W. Hell. Stimulated emission depletion microscopy with an offset depleting beam. *Applied Physics Letters*, 78(4):393–395, 2001. Compilation and indexing terms, Copyright 2007 Elsevier Inc. All rights reserved.

[16] http://www.picoquant.com/.

[17] Robert D. Frankel, Bruce W. Smith, and Andrew Estroff. Quantum state control interference lithography and trim double patterning for 32-16 nm lithography. In *Optical Microlithography XX*, volume 6520, page 65202, San Jose, CA, United States, Feb 27-Mar 2 2007 2007. Rochester Institute of Technology, Center for Nanolithography Research, Rochester, NY 14623-5603, SPIE, Bellingham WA, WA 98227-0010, United States. Compilation and indexing terms, Copyright 2007 Elsevier Inc. All rights reserved; T3: Proceedings of SPIE - The International Society for Optical Engineering.

[18] Claude Rullire. *Femtosecond laser pulses : principles and experiments.* Springer, Berlin ; New York, 1998. Claude Rullire, (ed.).; Bibliography: Includes bibliographical references and index.

[19] T. A. Klar. Progress in stimulated emission depletion microscopy, 2001.